

STUDY OF BEAM LOSSES DURING FAST EXTRACTION OF 800 GEV PROTONS  
FROM THE TEVATRON

A. I. Drozhdin and N. V. Mokhov  
Institute for High Energy Physics, Serpukhov USSR

and

M. Harrison  
Fermi National Accelerator Laboratory, Batavia, Illinois USA

May 1985

STUDY OF BEAM LOSSES DURING FAST EXTRACTION OF  
800 GeV PROTONS FROM THE TEVATRON

A.I.Drozhdin,<sup>1</sup> M.Harrison, N.V.Mokhov<sup>1</sup>

1. INTRODUCTION

The production of high intensity extracted beams from the new generation proton accelerators such as the Fermilab Tevatron, is limited primarily by radiation heating of the superconducting coils from beam losses in the accelerator structure. A low level of tolerable energy deposition in the superconducting coils<sup>[1-3]</sup> necessitates the use of special protection measures: magnetic sweeping (dog legs), multi-collimator systems, plugs inside magnets, etc. The optimization of these measures is generally done via Monte Carlo simulations. The projected rise of the energy and intensity of extracted proton beams at the Tevatron and the

---

1. Institute for High Energy Physics, Serpukhov, USSR

creation of the new accelerators, SSC, UNK, and LHC, increase the importance of such studies. In this paper we investigate the beam loss and quench problems in the Tevatron during fast extraction, calculationally and experimentally. We conclude with results obtained from a collimator-absorber system installed at D17 designed to significantly reduce the extraction losses in the ring.

## 2. CALCULATIONAL METHOD

We consider the situation in that half of the Tevatron ring, between the primary and secondary extraction septa from D0 up to A0, when during fast spill a part of the proton beam interacts with the electrostatic septum wires. The lattice and the geometric details are described elsewhere.<sup>[1]</sup>

The simulation of hadronic-electromagnetic cascades in the septum wires and in the downstream accelerator elements is done with the Monte Carlo program MARS10 developed from the code MARS9.<sup>[4,5]</sup> Having a 10 MeV-20 TeV working energy region this program is equipped with several new features: additive quark model for high energy hadron-nucleus interactions, a fast iteration-step geometrical module<sup>[6]</sup>

which is very convenient for constructing of three-dimensional hadron, electron and photon trajectories in the accelerator equipment with complicated geometry in the presence of magnetic fields, and an algorithm for multiple Coulomb scattering which is based on Moliere's theory with consideration of the finite extent of the nucleus.<sup>[7]</sup>

The flow of the calculation is as follows. With MARS10 we simulate the beam interactions with the first elements (electrostatic septa or the D0 straight section as a whole) and create a file of outgoing particles with energy greater than some limit,  $E > E_M = 0.8 E_0$ , for example, where  $E_0$  is the circulating proton energy. These particles are projected through each lattice element sequentially using the program STRUCT. Aperture checks are performed in each element and the particle distributions at the loss points are recorded. Then choosing places in the lattice where the loss level is high enough, the code MARS10 is again used to calculate the hadronic-electromagnetic cascades in the superconducting magnets and other elements in those locations.

The electrostatic septum model used in the calculation has two sections, 354.33 cm length with 85.73 cm space between, consisting of 75% tungsten and 25% rhenium wires of

0.002 inch diameter and 0.1 inch spacing with an angle of 25  $\mu$ rad between sections. The voltage setting is 93kV at 800 GeV so  $\vec{E}=83.036$  kV/cm. We have described as precisely as possible all details of the geometry of the septum and straight section downstream, the only approximation being an effective longitudinal density for the septum wires.

$$\rho_1 = \rho_0 \frac{0.002}{0.1} = 0.02 \rho_0, \quad |x| \leq a,$$

$$\rho_{\text{ef}} = \frac{2}{3} \rho_1, \quad a \leq |x| \leq 1.5a,$$

$$\frac{1}{3} \rho_1, \quad 1.5a \leq |x| \leq 2a,$$

where  $\rho_0 = 19.5$  g/cm<sup>3</sup>,  $a = 0.001$ ".

The equivalent magnetic field in the wires and in the space between wires and the cathode is

$$0, \quad x > 2a, \text{ or } x < -1.4 \text{ cm},$$

$$B_{\text{eq}} = 0.5 B_0 (1 - x/2a), \quad |x| < 2a,$$

$$B_0, \quad -1.4 \text{ cm} < x < -2a,$$

where  $B_0 = 0.3$  kG.

The beam parameters at the septum are

$$\begin{aligned}
y_0 &= y_0^1 = 0 \\
\sigma_y &= 0.7 \text{ mm}, \sigma_y^1 = 20 \text{ } \mu\text{rad}, \\
x_0^1 &= 160 \text{ } \mu\text{rad}, \sigma_x^1 = 8 \text{ } \mu\text{rad}, \\
\rho(x) &= \text{constant}.
\end{aligned}$$

Taking into account the geometry, the beam angle spread and the electrical field one can determine  $\delta$ -region from which protons can strike wires  $-0.1315 \leq x \leq 0.1358$  mm. This distribution is used to provide an absolute normalization to the results.

Number of protons:

<u>BEAM</u>	<u><math>\delta</math>-REGION</u>	<u>INTERSECT WIRES</u>
1	0.047	0.014
$2.13 \times 10^{12}$	$10^{11}$	$2.98 \times 10^{10}$

### 3. BEAM LOSS FORMATION DURING FAST EXTRACTION

In this section we present some of the calculational results which are of a general character and are used to optimize the protective measures.

The extracted beam phase space diagram at the upstream ends of the electrostatic septum and Lambertson magnet are shown in Figure 1. The septum wires are 14 mm from the closed orbit and the step size is 12 mm. The phase of extraction is such that the distance between circulating and extracted beam is equal to 6mm at the upstream end of Lambertson magnet at the start of the extraction channel. [8]

The next three plots illustrate the energetic characteristics of the source: electrostatic septum and D0 straight section as a whole. Figure 2 emphasizes the importance of precisely simulating all physical processes during high energy beam-septum interaction, even such as Landau fluctuation of ionization losses and fluctuations of the prompt  $e^+e^-$  pair production by protons. (The approximations can lead to the significant errors in the energy region of the candidates to be lost.) As seen from Figures 3, 4 there are no fast particles except the protons at the downstream end of the D0 straight section. Practically all of the neutrons, pions, and relatively slow protons have been captured in the dog-leg bump.

The horizontal phase space distribution at the downstream end of the straight section is shown in Figure 5.

One can see a two peaked structure in the x (radial) distribution that is the consequence of the septum shadowing effect.

To illustrate the predictive power of the code MARS10 we have reproduced all details of the geometry, material, and magnetic fields of the Tevatron for the first 60 meters from electrostatic septum up to first spool piece. The geometry and the positioning of beam loss monitors have been also put in the calculation. Figure 6 shows the absorbed dose in the loss monitors installed on the D0 elements. The beam intensity is  $\sim 10^{12}$  protons per fast spill. It is encouraging that the calculated dose and the readings in the detectors agree well. It is important to point out that loss monitor readings (absorbed dose) and the fast proton losses as calculated with any program start to correlate only in the relatively quiet region, after D0 bump for example.

A snapshot of the ring-wide loss distribution taken during fast spill is shown in Figure 7. The losses are spread out around the ring at locations where the phase of the scattered beam is such that particles are lost from the machine aperture. In operational terms the beam losses at

the high-beta region at F49 were sufficient to limit the intensity of a fast extracted beam pulse to  $\sim 2 \times 10^{12}$  to avoid quenching the quadrupoles in this region.

In order to improve this intensity limitation we set out to see whether it would be possible to devise a collimation scheme which would be capable of affecting the loss distribution significantly without quenching the elements closest to the collimators. The cryogenic nature of the environment restricts possible collimator locations to the warm regions of the machine (straight sections, 17 and 48 locations).

The radial distribution of the extracted and scattered beams together with the projected machine aperture are shown in Figure 8 for the first three possible collimator locations (D0, D17, D48) and the critical aperture at F49. Comparing these distributions one can see that the D17 location allows the largest range of possible collimator setting without limiting the extracted beam aperture.

Calculated beam loss distributions around half of the ring are shown in Figure 9 for two different collimator settings at D17 and D48. This data is calculated for an ideal (linear) machine with a perfect closed orbit. The

vertical lines correspond to the number of protons lost on each element rather than loss monitor readings. Changes in the loss distributions are apparent.

The next step was to install the actual high field orbit as given in Figure 10. This was accomplished by turning on dipole correction elements placed after each focussing quadrupole. Figure 11 shows the corresponding results for various collimator settings; one should note the reduction of F49 losses as the collimators move further into the aperture.

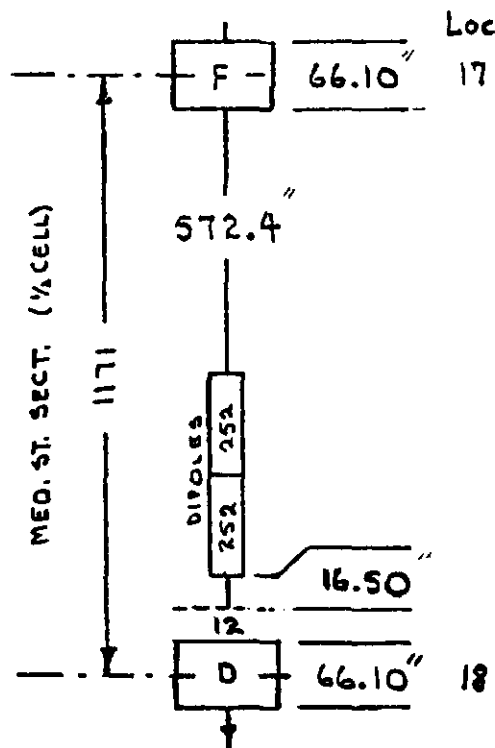
The final step in this part of the calculation involved turning on the non-linear dipole fields. This was done by randomly generating field harmonics of the appropriate distributions in each magnet. Three situations: without non-linearities, with non-linearities, and with non-linearities increased by a factor of 5, are shown in Figure 12. The real non-linear fields have a minimal effect on the loss distributions.

#### 4. BEAM LOSS LOCALIZATION AT D17

From the results of the previous section one can see that collimators can be used to influence the ring-wide loss

distribution and the dynamics of fast extraction are such that D17 represents the optimum location for such a system. Localizing the losses in this area however requires that the nearest superconducting magnets are protected against the secondary radiation produced from the collimators themselves.

To this end we have made a number of MARS10 runs for a variety of different collimator and secondary absorber layouts in the D17 region. We also investigated the possibility of using plugs in the nearest superconducting dipole. The layout of the cold elements in the D17 location is shown below.



The results of these runs are summarized in Table I.

The collimators used in these simulations were L-shaped stainless steel devices, 5 cm thick and of variable lengths as indicated. The absorbers and dipole plugs were also stainless steel of various thicknesses. The loss data is presented in terms of total energy deposited in the first two downstream superconducting dipoles as well as the maximum energy deposition in the superconducting coils. All these results correspond to  $2 \times 10^{12}$  protons per fast spill. We also consider cases with plugs inside the first dipole, the values of energy deposited in them is shown in the table too. For 800 GeV and the nominal operating temperature (4.6°K) the quench level of a dipole lies in the 1-4 mJ/g range.

Run numbers 10→13 correspond to the final design with a long collimator installed at the beginning of the drift space and two "thick beam tubes" (absorbers) downstream.

One can see from Table I that the best results are obtained from run #11, comparing this data with run #1 (two short collimators and no absorbers) the maximum energy density is decreased by a factor of ~40, total energy in the first dipole by ~13 and the second dipole by ~5.

The longitudinal distribution of the energy density deposited in the superconducting coils is shown in Figure 13. One can see how the upstream end of the first dipole is effectively shielded by the absorbers. The radial distribution of deposited energy density at the shower maximum is shown in Figure 14. The radial gradient is similar to unshielded magnets (D16 dipoles for example). At the same time, the energy deposition in the front face of the first dipole coil shows little radial dependence. The azimuthal distribution of energy deposition around the coil of the shielded dipole is also more uniform than in the unshielded ones.

The best results from Table I are obtained from run #11. This layout has a long (160 cm) collimator followed immediately by an absorber (inner radius 2.3 cm, outer 6.0 cm) with a second absorber (inner radius 2.5 cm, outer 6.0 cm) upstream of the first dipole. The absolute value of the energy density maximum ( $\sim 0.01$  mJ/g) is well below the quench threshold but is obviously strongly dependent on the position of the collimators relative to the closed orbit, so one should take this more as a variable parameter than a fixed result.

## 5. EXPERIMENTAL RESULTS

These calculations were considered sufficiently encouraging that the decision was made to install a collimator system identical to that used in run #11. Since that time two study sessions (one parasitic, one dedicated) were devoted to investigating the effect of the system on fast extracted beam loss. The first session (parasitic) was used to align the collimator to the beam and then slowly move the aligned collimator in small steps (0.5 mm) into the beam at low intensity ( $3 \times 10^{11}$  per fast spill). The second session was devoted to raising the intensity of the fast spill.

The results of the first session are summarized in Figures 15 and 16. Figure 15 shows the ring-wide loss distribution with the collimator out of the beam. Comparing this to Figure 7 one can see that even without the collimator the absorbers themselves are limiting the aperture sufficiently to start affecting the loss distributions. The non-zero reading on the D18 loss monitor attests to this fact. With the collimators installed 16 mm from the closed orbit position the loss distribution is as given in Figure 16. The results are dramatic when compared

with Figure 7. The losses in sectors D, E, and F are all reduced, especially in the "quenching" region at F49 where a factor of ~30 reduction is shown. These changes in the loss patterns should be compared to the predictions given in Figure 9 for example, the qualitative agreement is good.

Loss distributions as a function of collimator position are shown in Figure 17 together with the predicted response for three locations in the ring. The overall normalization of the measured data is arbitrary but again one can see excellent agreement between the calculations and the data.

The second study session was devoted to raising the intensity of the fast spill. Starting at  $1 \times 10^{12}$  the intensity was slowly raised until slightly over  $1 \times 10^{13}$  was extracted without quenching the accelerator. At this point no more intensity was available so the results are somewhat inconclusive in terms of establishing a quench threshold but nevertheless the collimator system appears to have reduced the beam loading on the magnets to the point that a five-fold increase in fast extracted beam spill intensity has been achieved.

## CONCLUSIONS

The installation of a collimator-absorber system in the Tevatron has been successful in reducing the effect of fast extracted beam losses in the cryogenic elements.

Excellent agreement between the Monte Carlo calculations and the experimental observations are encouraging with a view to future accelerators.

## ACKNOWLEDGEMENTS

The authors wish to thank Don Edwards and David Finley for their assistance in various aspects of this report. Two of us, A. Drozhdin and N.Mokhov, would like to thank the Fermilab Accelerator Division for the hospitality shown during their recent visit.

## REFERENCES

1. Superconducting Accelerator, Design Report, Fermilab, 1979.
2. M.A.Maslov, N.V.Mokhov, Particle Accelerators, V. 11, 91, 1980.
3. M.A.Maslov, N.V.Mokhov, in Proc. III ICFA Workshop, p.3, Protvino, 1981.
4. N.V.Mokhov, preprint IHEP 82-168, Serpukhov, 1982.
5. A.N.Kalinovsky, N.V.Mokhov, Yu. P.Nikitin, "Penetration of High Energy Particles Through Matter," Moscow, Energoatomizdat, 1984.
6. M.A.Maslov, N.V.Mokhov, preprint IHEP 85-8, Serpukhov, 1985.
7. I.S.Baishev, N.V.Mokhov, S.I.Striganov, preprint IHEP 84-210, Serpukhov, 1984, to be published in "Yadernaya Physica."
8. M.Harrison, Extraction III-Fast Resonant Extraction, Fermi National Accelerator Laboratory, UPC No. 87, February 27, 1979.

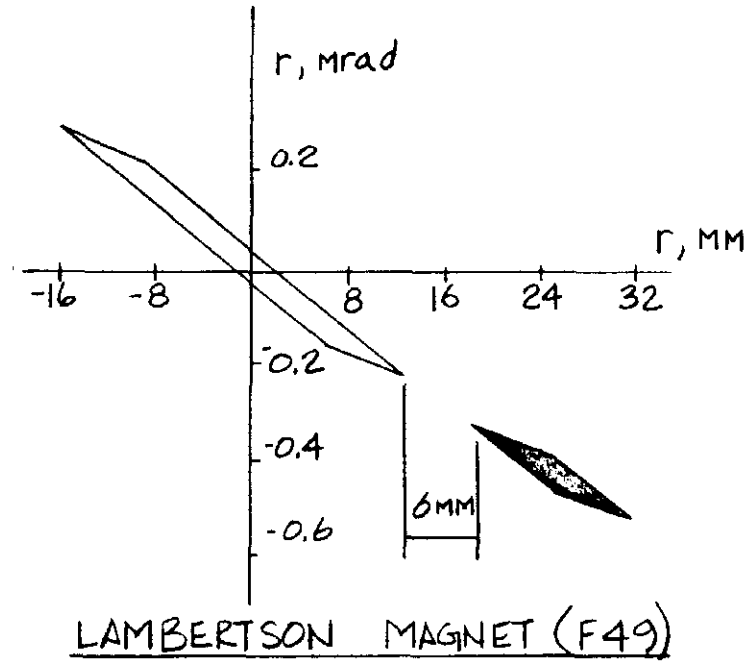
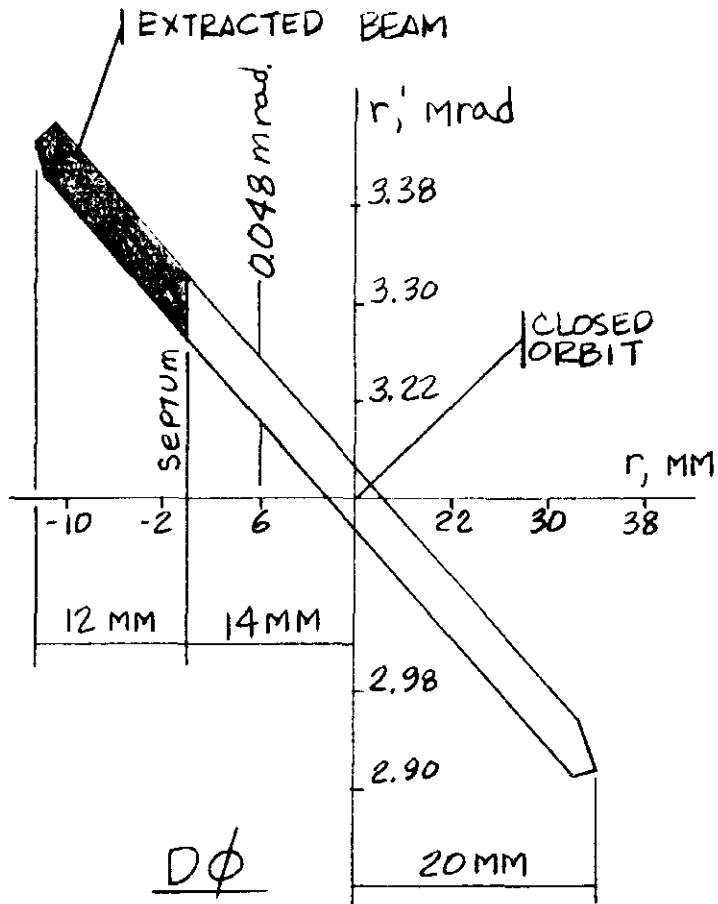


FIG. 1

EXTRACTED BEAM PHASE SPACE DISTRIBUTION AT THE EXTRACTION SEPTA

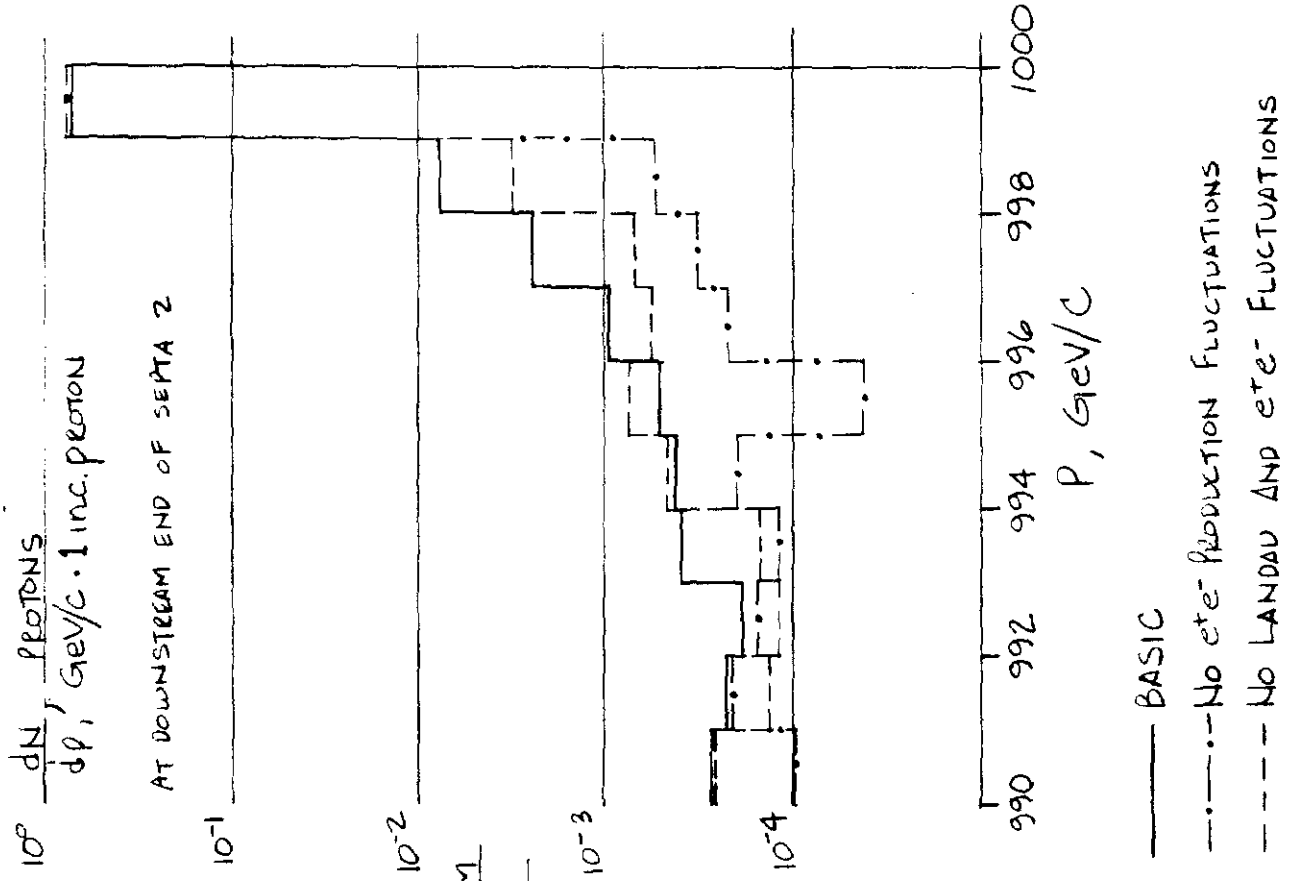


FIG. 2  
SMALL ANGLE ELASTICS FROM  
THE ELECTROSTATIC SEPTUM

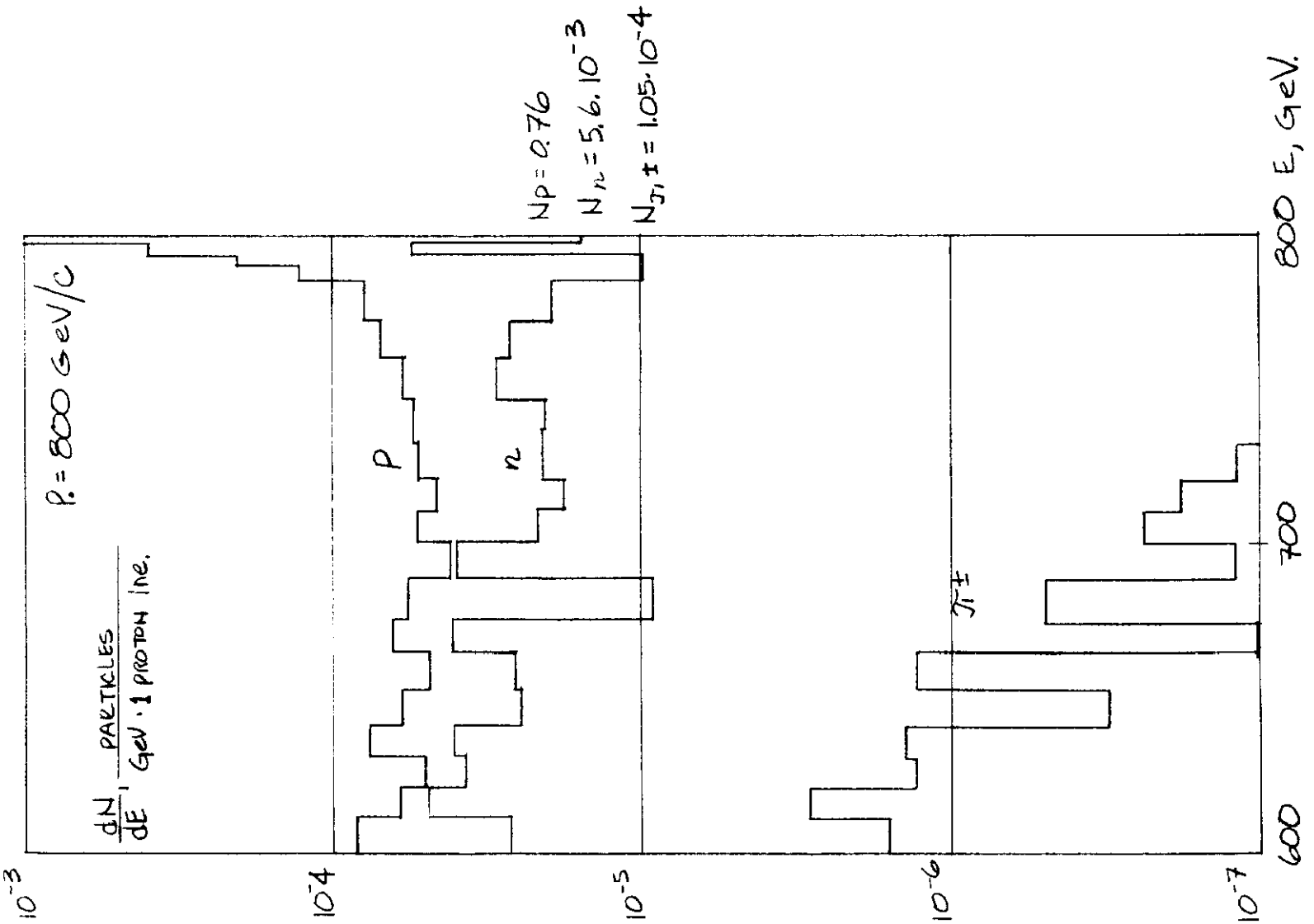


FIG. 3  
PARTICLE PRODUCTION  
FROM ELECTROSTATIC  
SEPTUM

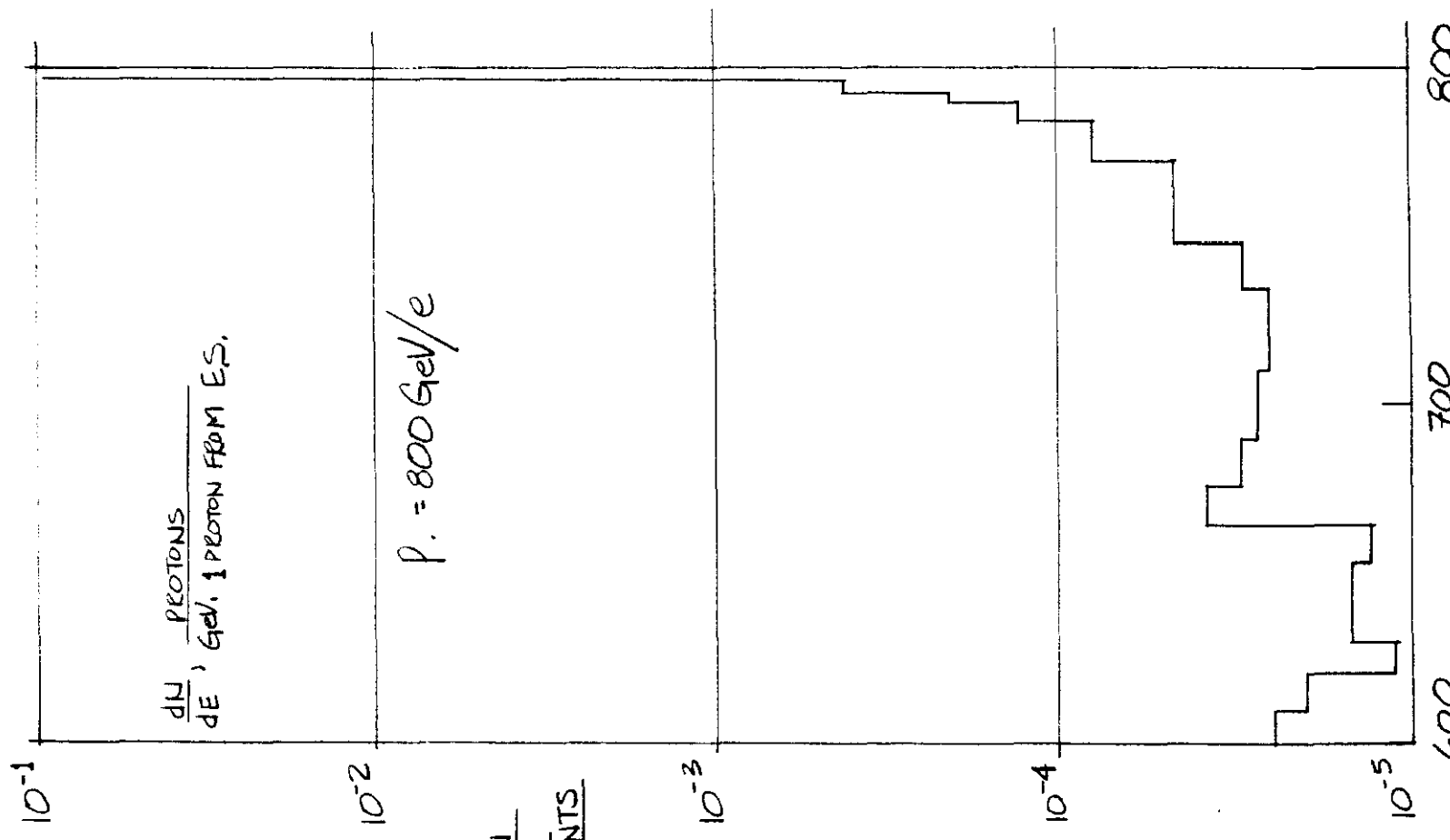


FIG. 4  
PARTICLE DISTRIBUTION  
AT THE START OF THE  
SUPERCONDUCTING ELEMENTS

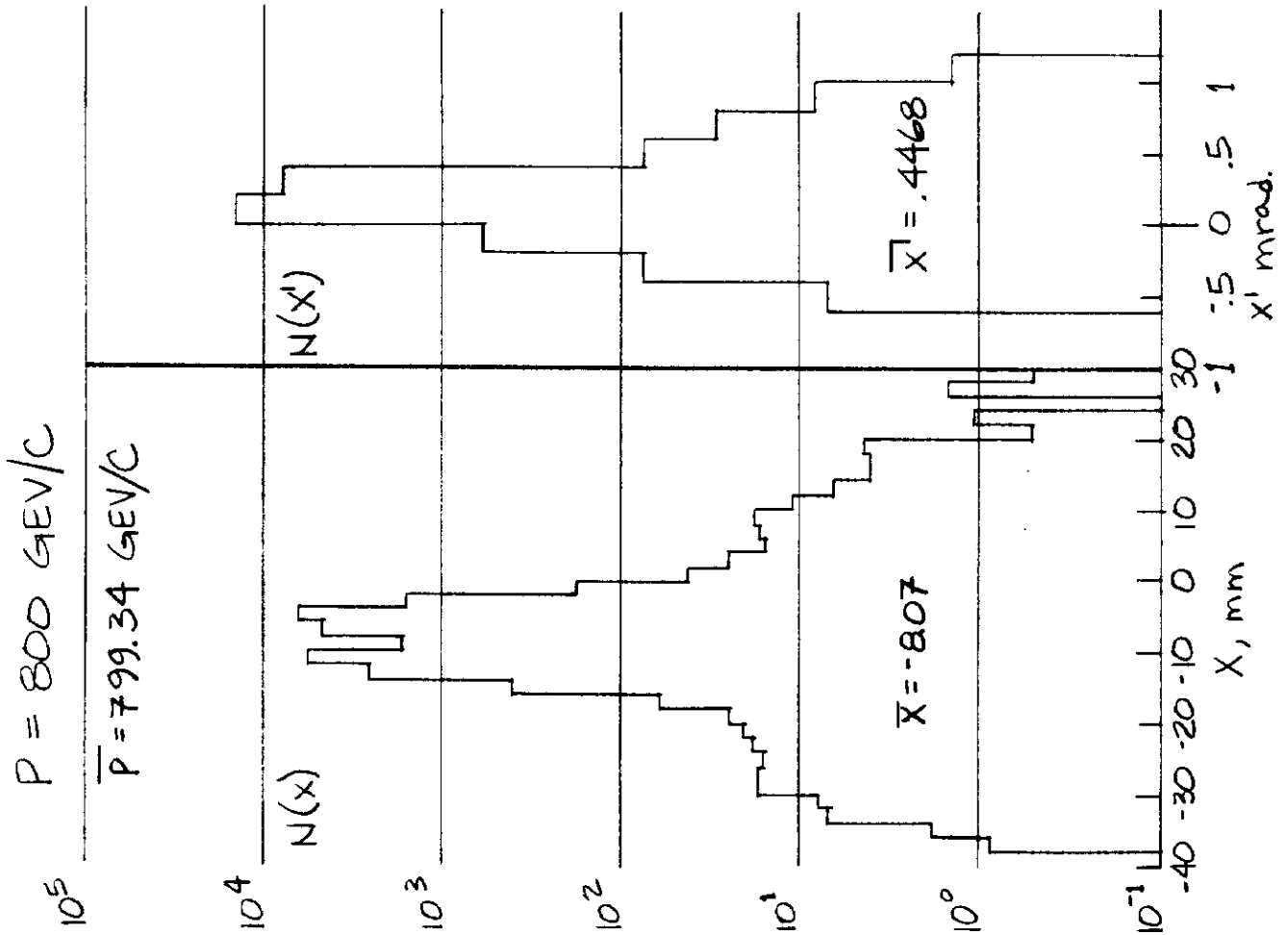


FIG. 5  
PHASE SPACE DISTRIBUTION AT THE START OF THE SUPERCONDUCTING ELEMENTS.

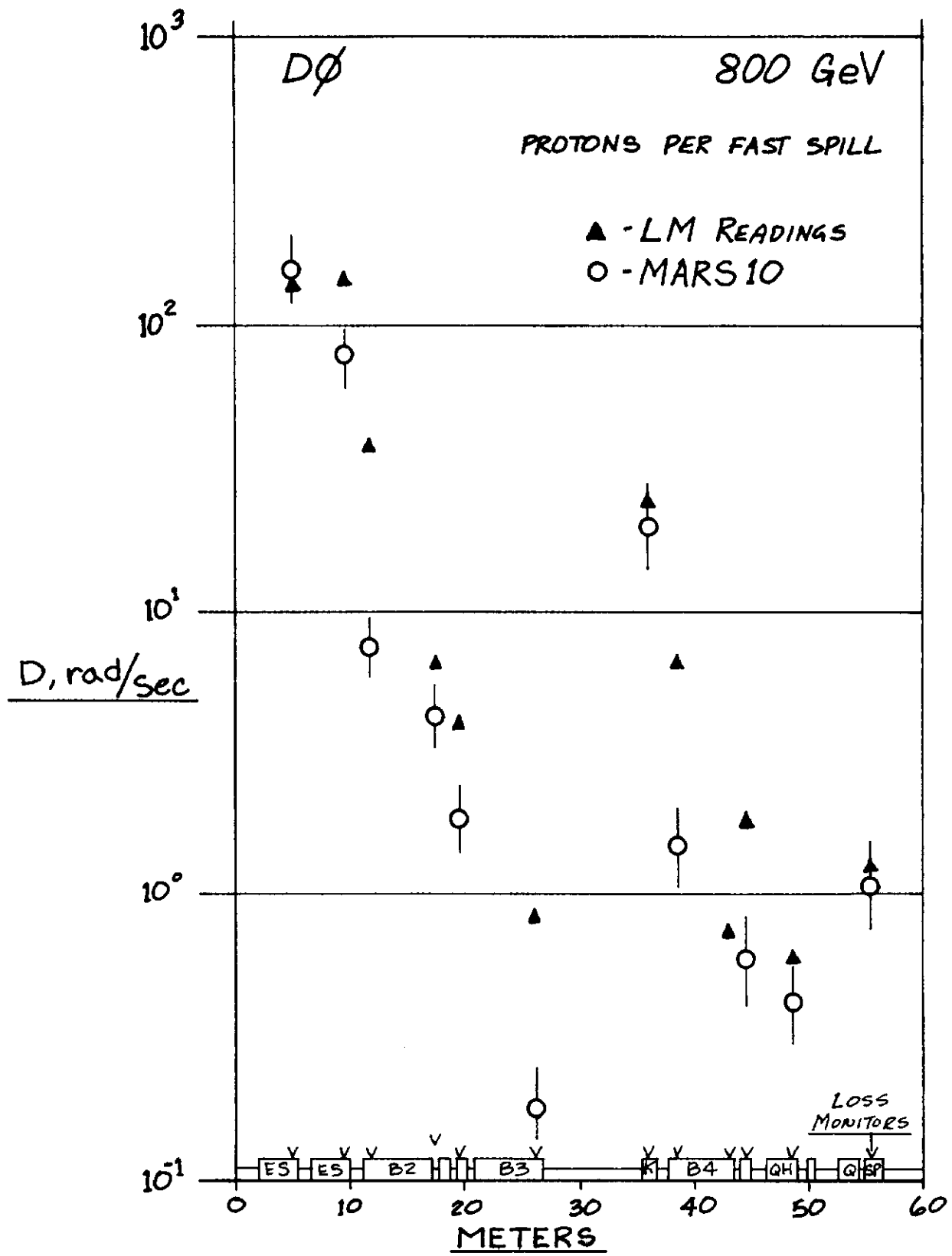


FIG. 6

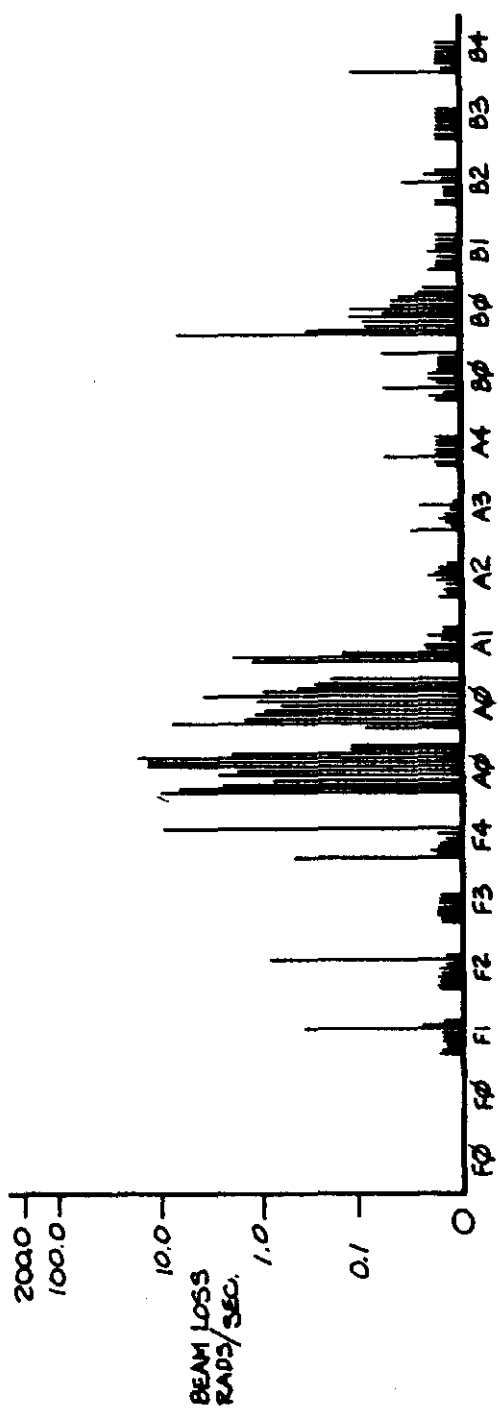
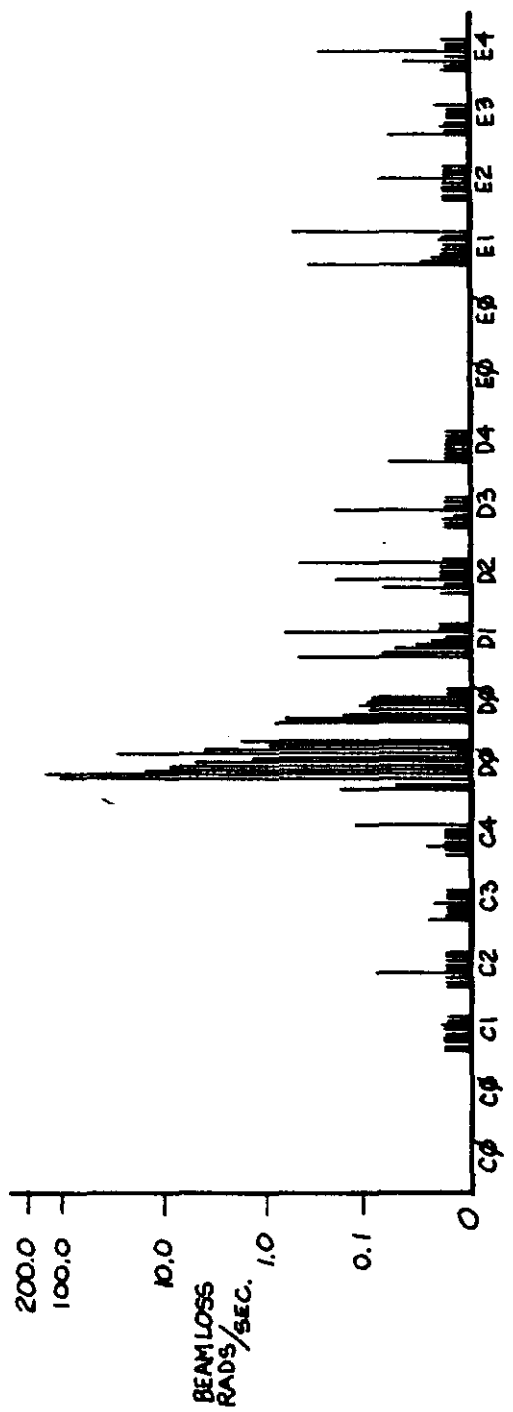


FIG. 7 RING WIDE FAST EXTRACTION LOSSES WITH NO COLLIMATION

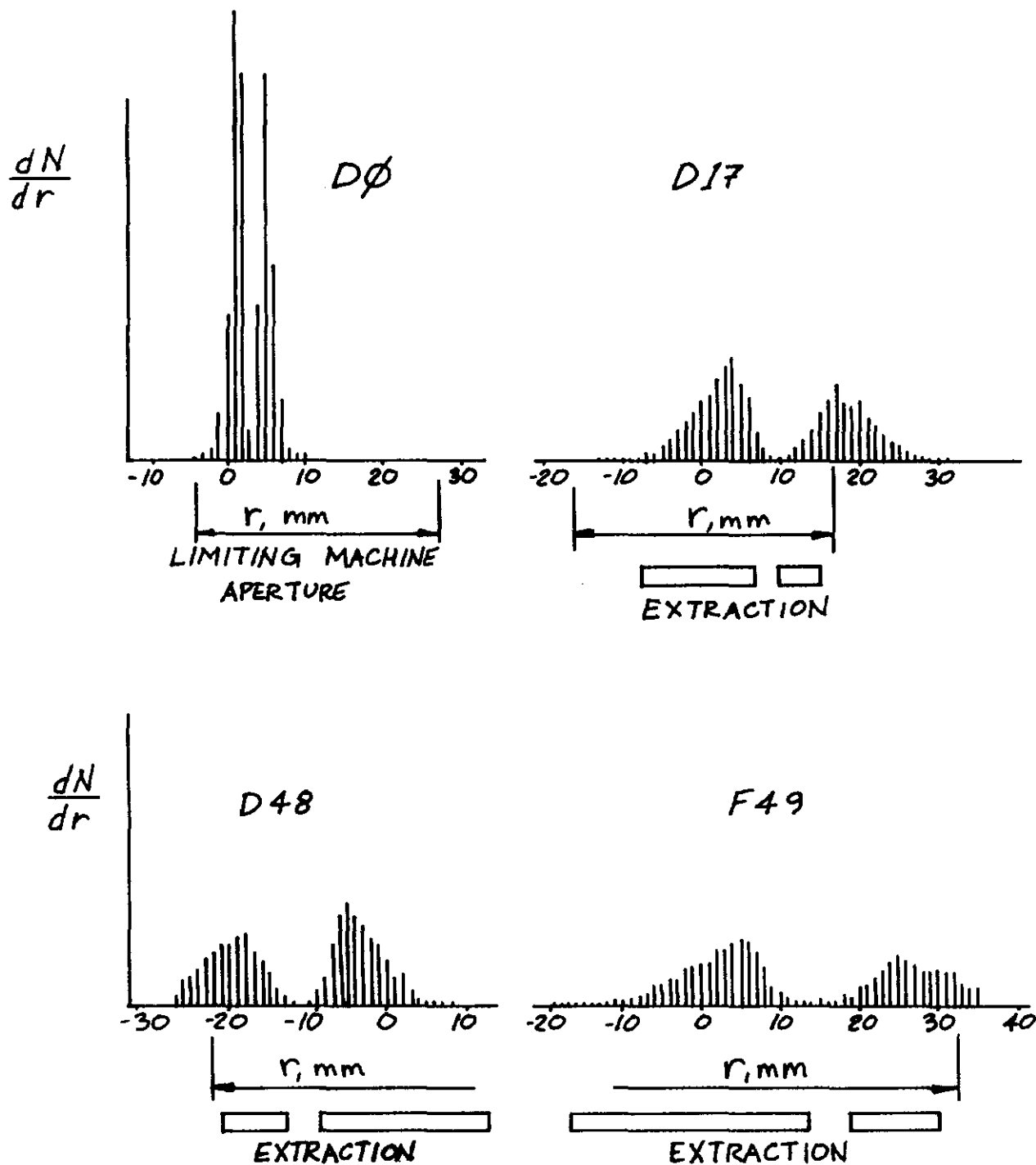


FIG. 8

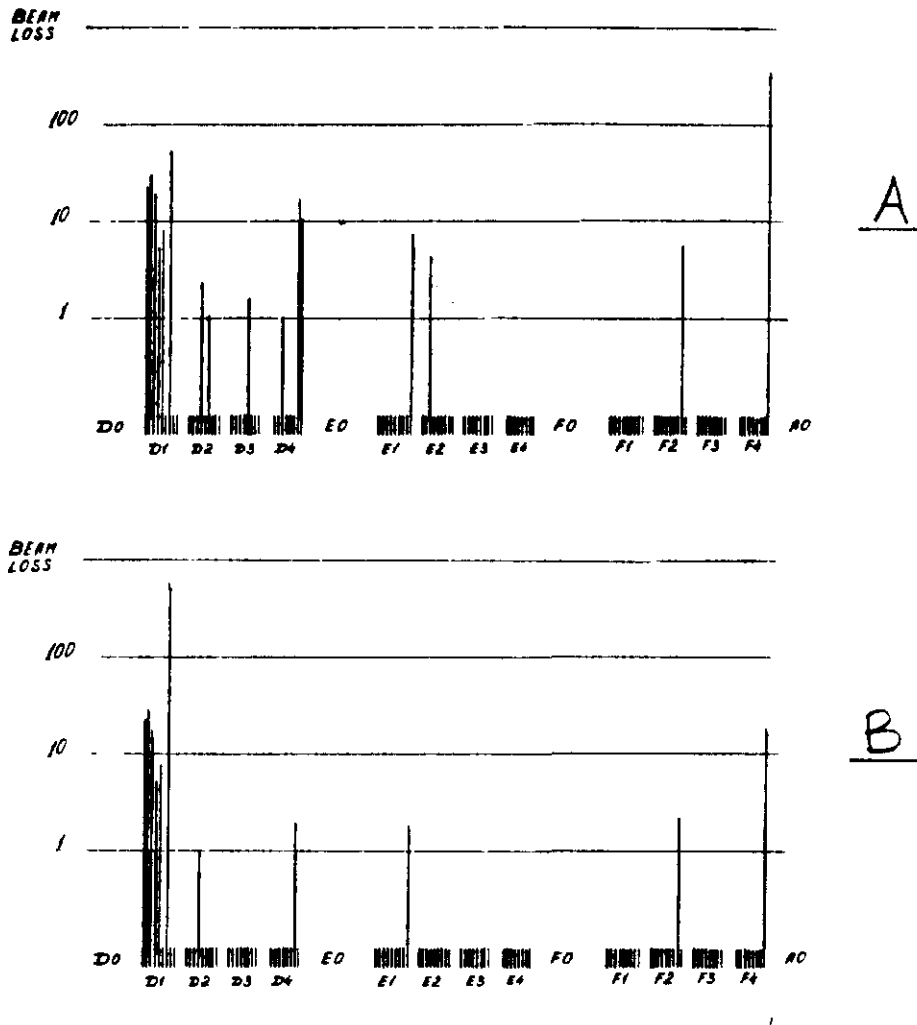


FIG. 9

BEAM LOSS NOMINAL CLOSED ORBIT

- A) COLLIMATORS AT  $\pm 25$  mm
- B) DIF COLLIMATORS AT  $+ 16$  mm

	(MM)				04-15/85 1408	
	C	D	E	F	A	B
11	-.61	-1.23	7.12	.03	1.9	.14
13	.25	-.61	-.1	.4	2.09	-.34
15	.27	-.96	-.11	.42	2.48	-.17
17	.12	-4.1	.16	.4	.05	-.05
19	.15	-.28	.08	-.01	.12	.38
22	-.29	-.03	-.1	-.25	.2	-.34
24	.07	-.07	.13	.3	.42	.12
26	.12	.07	.15	.52	.38	0
28	-.17	-.18	-.1	-1.03	.22	.22
32	.12	-.06	.1	0	.21	.2
34	-.07	-.05	.27	-.13	-.3	.04
36	.03	2.92	-.19	.02	-.1	-.55
38	.37	.15	-.1	.38	.05	-.06
42	.37	.03	-.08	-1.89	.17	-.01
44	.05	NOBEAM	.37	.26	0	.5
46	-.34	.24	-.1	-.29	-.25	.18
48	.89	3.25	.21	-2.94	-.68	-.47
49	-1.46	5.15	.18	-.51	.06	-.31

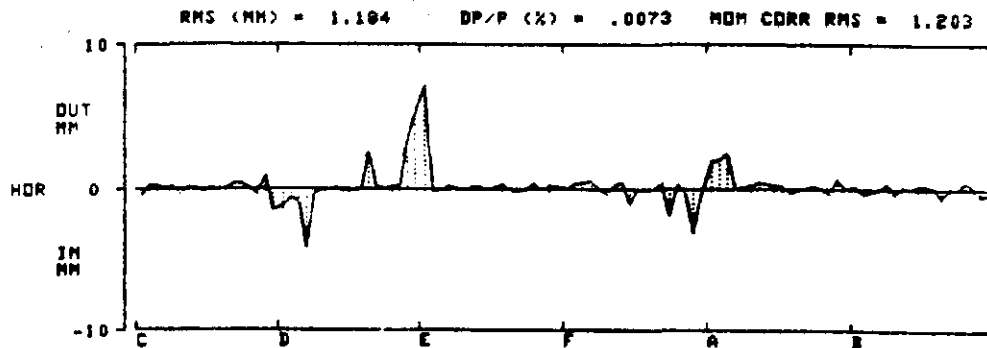
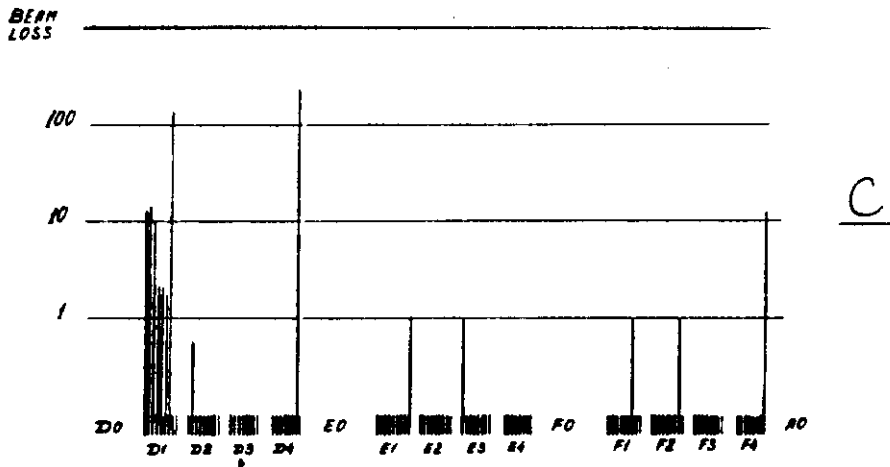
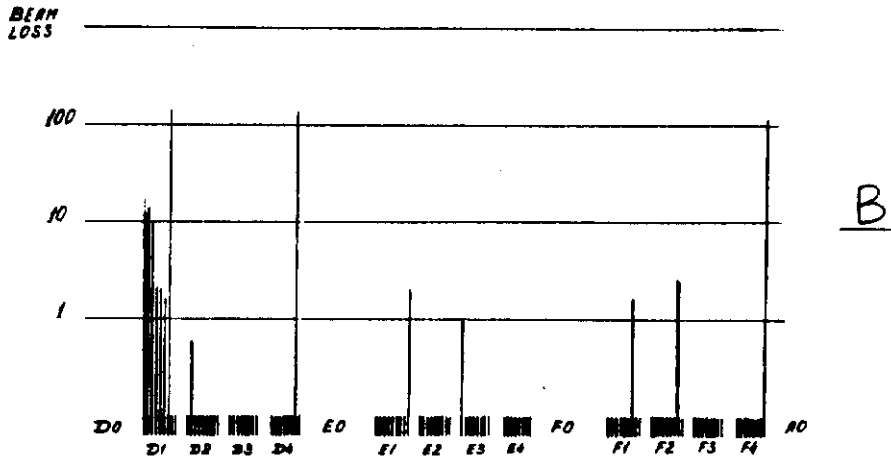
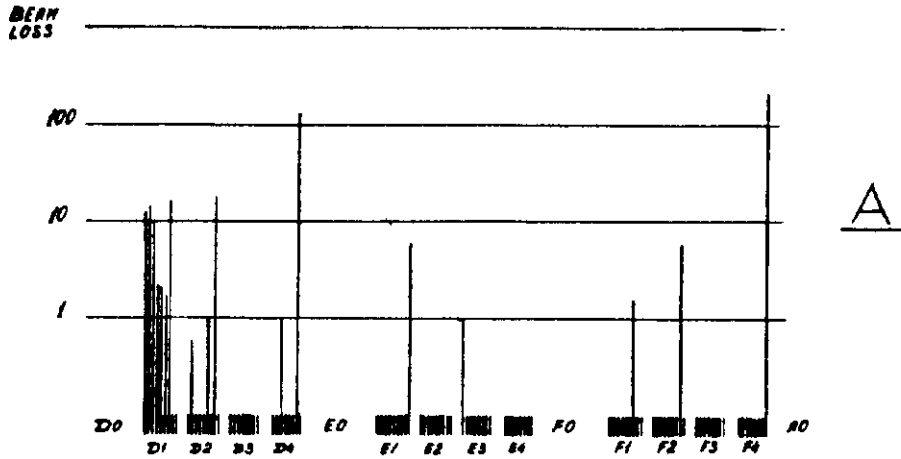


FIG. 10

HIGH FIELD HORIZONTAL CLOSED ORBIT

# FIG. 11

## BEAM LOSS REAL CLOSED ORBIT



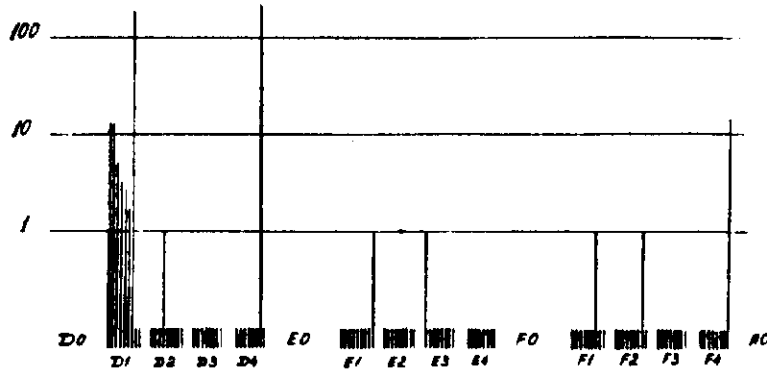
- A) ALL COLLIMATORS AT  $\pm 25.4$  mm
- B) D17 AT 16.5 mm, D48 AT -23.4 mm
- C) D17 AT 16.5 mm, D48 AT -22.4 mm

FIG. 12

BEAM LOSS NONLINEAR DIPOLE FIELDS

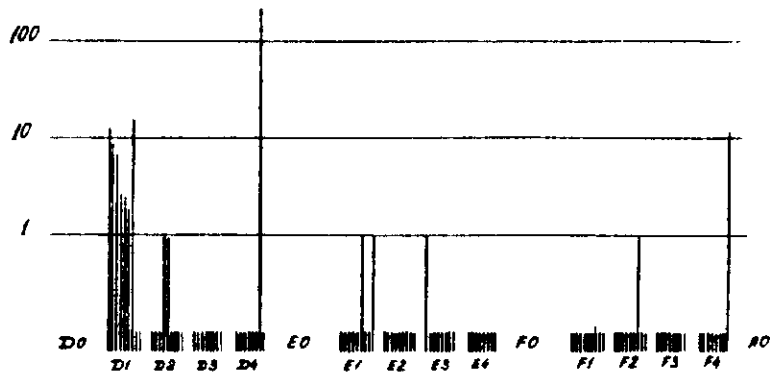
D17 COLLIMATOR AT 16.5 mm  
D48 COLLIMATOR AT 22.4 mm

BEAM  
LOSS



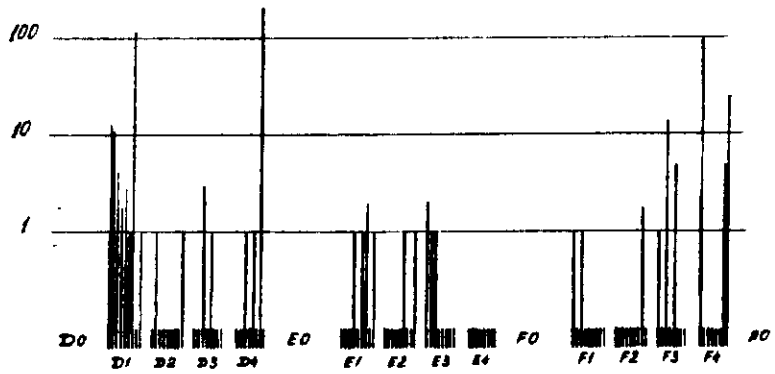
A

BEAM  
LOSS



B

BEAM  
LOSS



C

- A) WITHOUT NONLINEARITIES
- B) WITH NONLINEARITIES
- C) WITH 5X NONLINEARITIES

TABLE 1

Run #	Collimators			Absorbers $\ell_{A1}/\ell_{A2}$	Dipole 1 Plug	Dipole 1			Dipole 2		
	$\Delta_1/\Delta_2$	$Z_1/Z_2$	$\ell_1/\ell_2$			$E_T$	$E_D$	$\epsilon_{max}$	$E_T$	$E_D$	$\epsilon_{max}$
1	1.8/1.8	$\frac{1130.94}{1009.02}$	63.5/63.5	No	No	14.	252.	.32	1.8	18.4	.04
2	-1-	$\frac{1009.02}{1130.94}$	-1-	No	No	11.	158.	.25	1.7	18.1	.04
3	-1-	-1-	-1-	No	$R_i=1.8$	4.5	110.7	.35	.4	2.2	.006
4	-1-	-1-	-1-	No	$R_i=2.54$	5.7	133.	.27	1.1	10.3	.01
5	-1-	$\frac{915.02}{1130.94}$	157.5/63.5	No	$R_i=2.54$	2.5	52.	.063	.46	3.9	.002
6	-1-	-1-	-1-	No	No	4.3	82.	.083	.8	5.6	.009
7	2.29/1.9	$\frac{75.57}{197.49}$	63.5/63.5	No	No	3.1	76.4	.092	1.	11.5	.017
8	-1-	$\frac{75.57}{291.49}$	157.5/63.5	No	No	1.2	40.5	.047	.5	5.6	.011
9	-1-	$\frac{75.57}{1130.94}$	63.5/63.5	No	No	3.	63.5	.09	1.2	13.6	.018
10*	2.29	75.57	157.5	75/225	No	.56	24.1	.015	.38	4.61	.01
11*	-1-	-1-	-1-	75/150	No	.41	19.7	.008	.3	3.8	.006
12**	-1-	-1-	-1-	-1-	$R_i=2.54$	.41	20.5	.009	.25	2.74	.002
13***	-1-	-1-	-1-	-1-	No	.89	32.4	.034	.43	4.0	.007

(continued)

All dimensions are in centimeters.  $E_T$  and  $E_D$  is energy deposited in the beam tube and in the remaining dipole ( $r > 3.81$  cm) in GeV per one incident 800 GeV proton on C1 + C2.

$\epsilon_{max}$  is the maximum energy deposition density in the dipole superconducting coil in mJ/gm per  $2 \times 10^{12}$  protons per fast spill.

\* A1:  $R_i = 2.54$  cm, A2:  $R_i = 3$  cm,  $R_{out} = 6$  cm

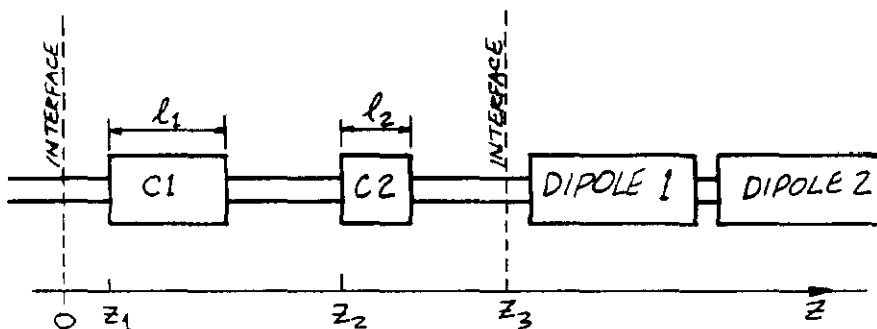
\*\* Runs No. 11-12:

A1:  $R_i = 2.29$  cm, A2:  $R_i = 2.54$  cm,  $R_{out} = 6$  cm

\*\*\* in Run No. 13:

A1:  $R_i = 2.29$  cm, A2:  $R_i = 2.54$  cm,  $R_{out} = 3.81$  cm

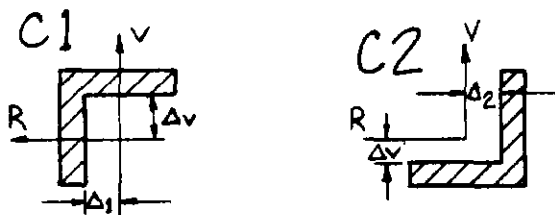
RUNS NO.  
1-9



NOT TO SCALE  
ALL DIMENSIONS IN CM.

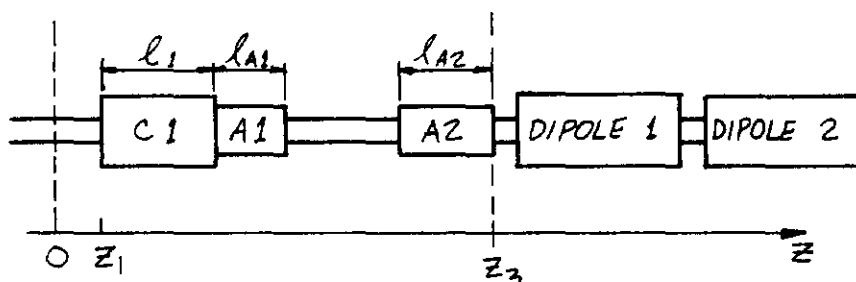
$z_3 = 1280.16$  cm.

JAWS POSITION



$\Delta v = 2.54$  cm

RUNS NO.  
10-13



ABSORBOR OUTER RADIUS,  $R_A = 6$  cm.

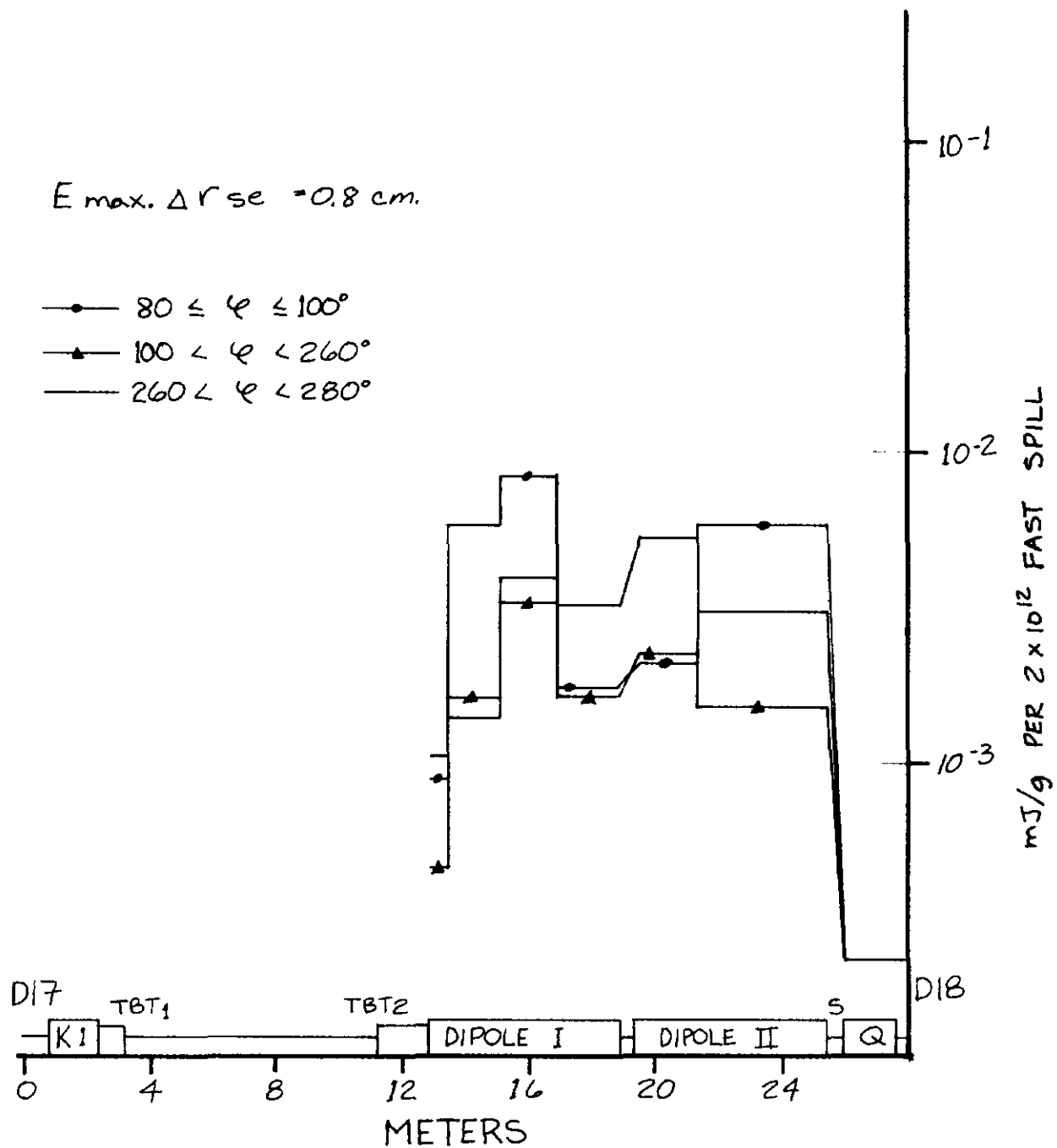


FIG. 13  
LONGITUDINAL VARIATION OF DEPOSITED ENERGY DENSITY IN THE SUPERCONDUCTING COILS.

800 GEV D17 DIPOLE I

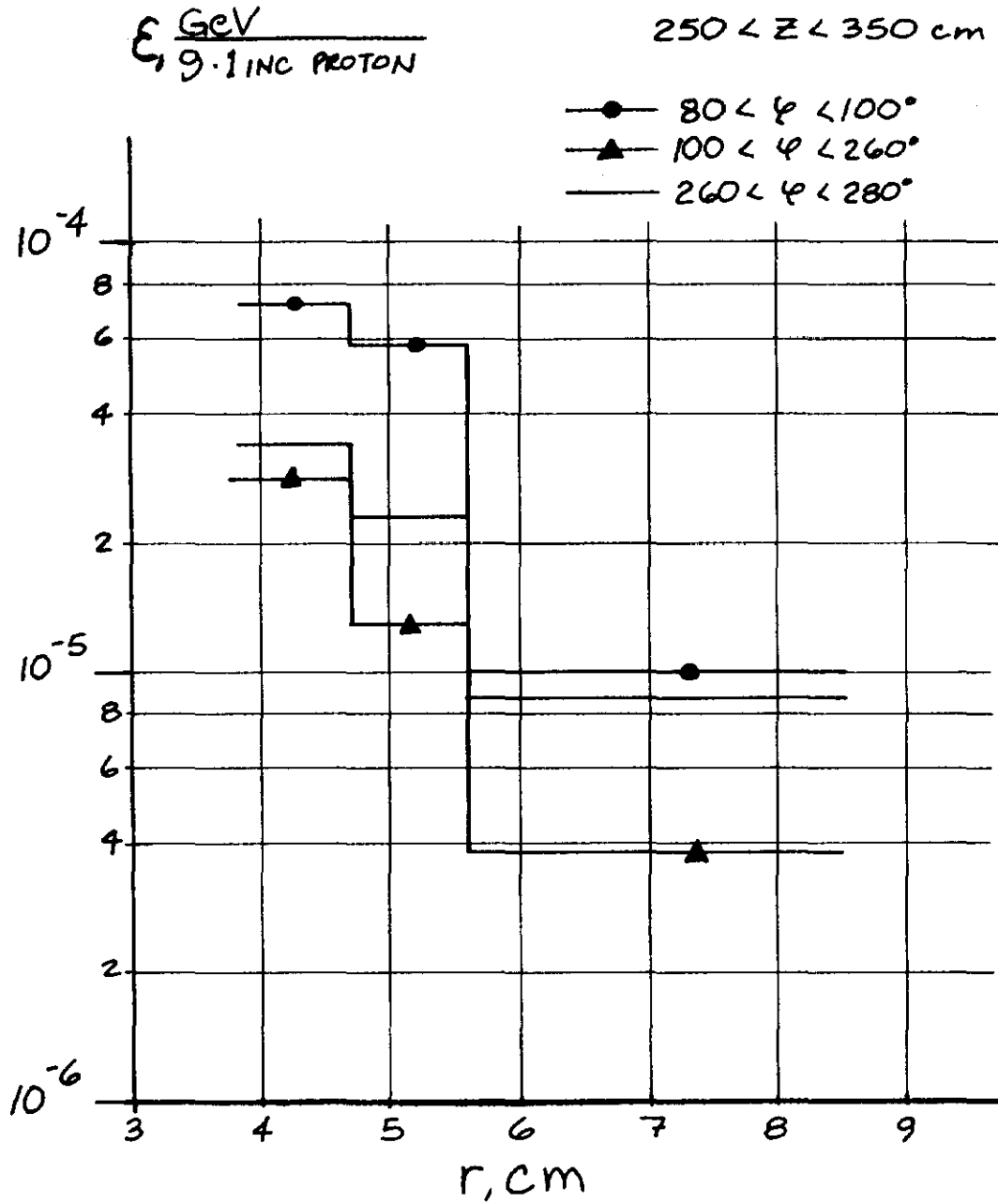


FIG. 14

RADIAL DISTRIBUTION OF DEPOSITED ENERGY  
DENSITY AT THE SHOWER MAXIMUM

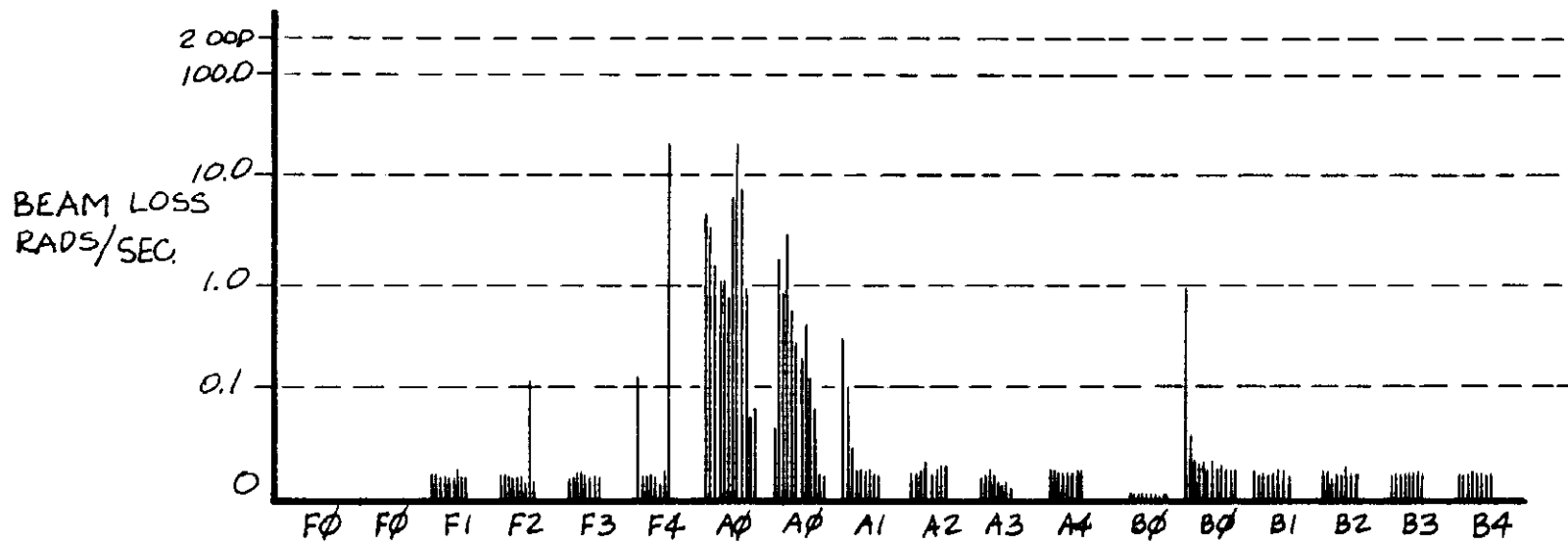
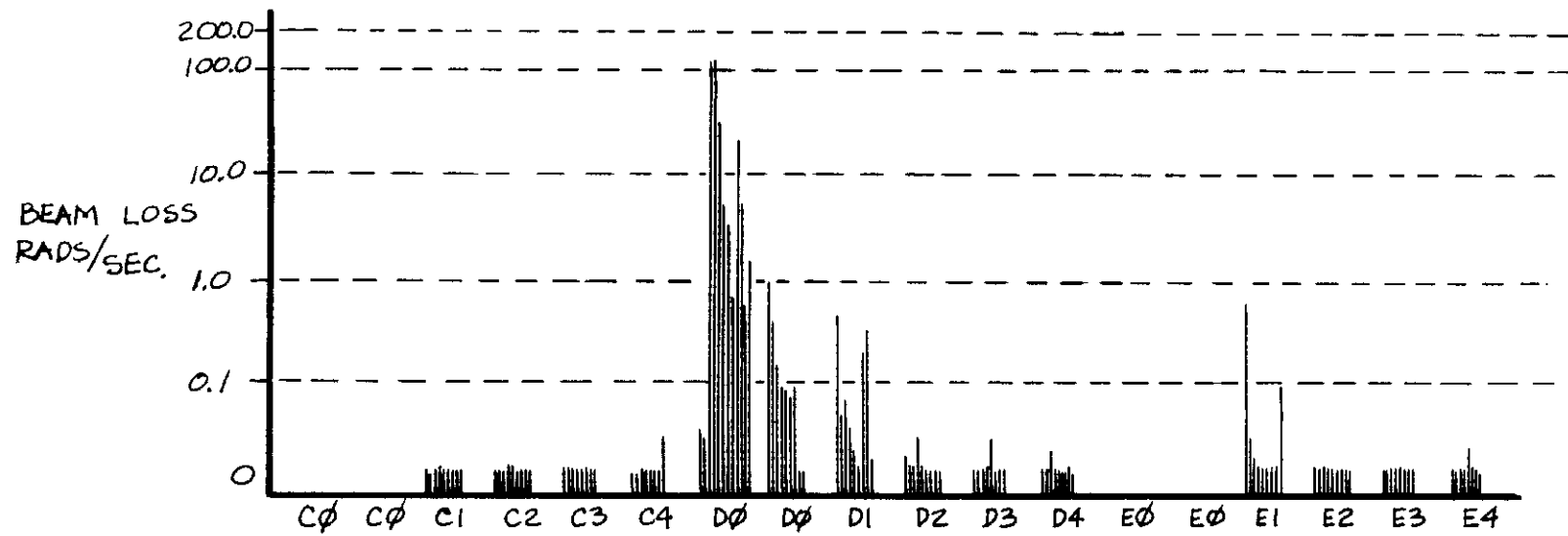


FIG. 15

RING WIDE FAST EXTRACTION LOSSES  
COLLIMATOR OUT OF BEAM

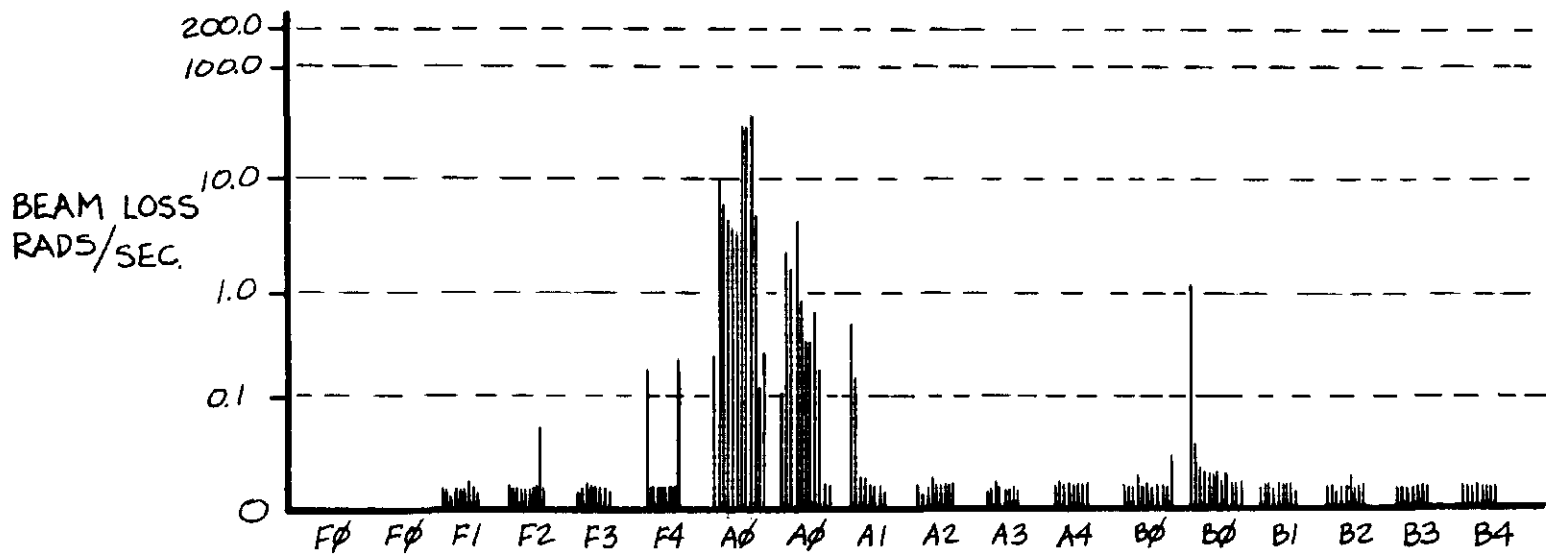
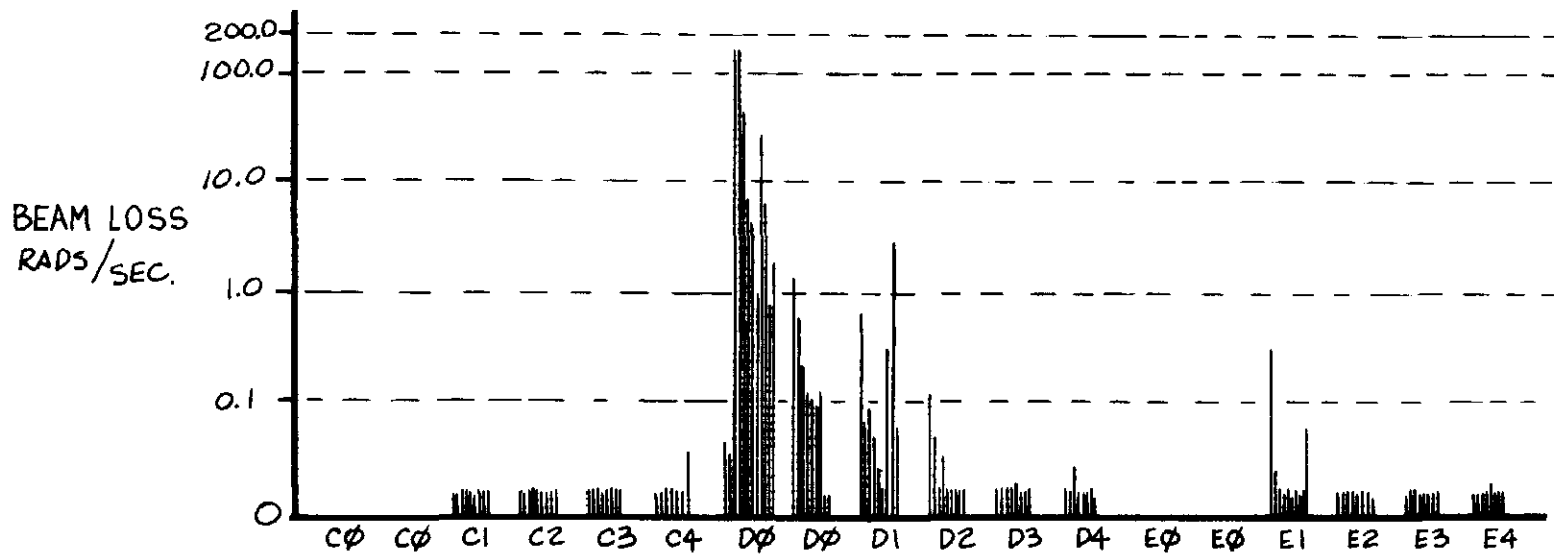


FIG. 16

RING WIDE FAST EXTRACTION LOSSES WITH COLLIMATION

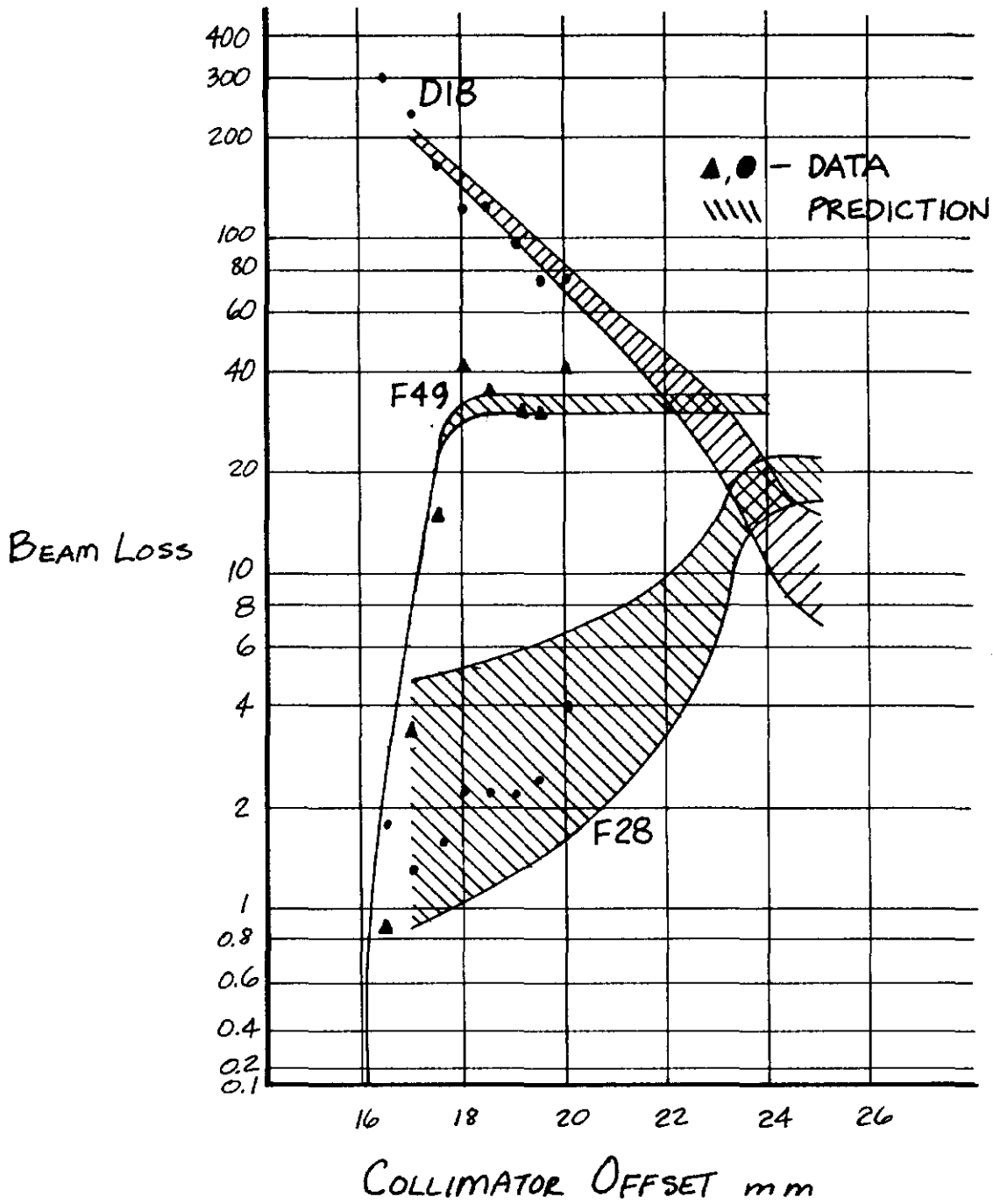


FIG. 17

BEAM LOSS V'S COLLIMATOR POSITION PREDICTION  
AND RESULTS FOR LOCATIONS D18, F28, F49